

*Marco Gabella^{1,2}, Efrat Morin§¹MeteoSwiss, Locarno Monti, Switzerland²Dipartimento di Elettronica, Politecnico di Torino, Italy

§Department of Geography, Hebrew University of Jerusalem, Jerusalem, Israel

1. INTRODUCTION

Ground-based and TRMM precipitation radars provide a complementary view: the Ground-based Radar (GR) measures rain from a lateral direction, while the TRMM radar sees it from the top. There are enormous differences between these two instruments. Mention can be made of the different operation frequencies, sampling volumes, geometrical viewing angles, attenuation, sensitivity and times of acquisition. Consequently, a quantitative comparison between TRMM Precipitation Radar (TPR) and GR is a challenge, as can be seen for instance in Bolen and Chandrasekar (2003).

Shape and size of the sampling volumes of the two radars at the same location are different. However, the fact that different ranges and viewing angles cause such significant differences represents also an opportunity: by averaging many echoes in a given region, it is possible to use the quasi-orthogonal and independent view of one sensor for checking the observations of the other one.

2. THE CONCEPT

Among many esteems of the TPR, one is certainly represented by its long-term, continuously monitored electronic stability. The calibration factor is assumed to have a remarkable accuracy: its uncertainty is smaller than 1 dB. Consequently, the TRMM Precipitation Radar (TPR) provides the possibility of assessing the average bias of ground-based radars around the world. Quantitative assessments of this kind have been performed, e. g., in Florida (Liao et al., 2001), Colorado (Bolen and Chandrasekar, 2003), Marshall Islands (Houze et al., 2004), Australia (Keenan et al., 2003) and Cyprus (Gabella et al., 2006a). In the latter case, a novel comparison between the TPR and the GR was also suggested, based on the fact that such radars provide a complementary view: the (GR) measures rain from a lateral direction, while the space-borne radar sees it from the top. On the one hand, the lateral GR measurements are used for quantitative precipitation estimation at distances between 10 km (or even less) and 100 km (or even more). Because of this large ratio of distances, the scattering volume changes by a factor of over 100, since the volume increases with the square of the distance.

On the other hand, the scattering volume of TPR has a similar size in all the locations. Its size is little correlated to the distance between the echo and the GR. This advantage of TPR stimulated the idea of using TRMM radar to estimate the influence of sampling volume of the ground-based radar.

2.1 TRMM-derived range-adjustment of the GR

Our analysis is based on the average radar-derived rainfall intensity (in circular rings around the GR site) as a function of the distance, d , from the GR site. The lateral GR measurements are limited, in the present study, at distances between 10 and 110 km. For both radars, we compute the average rainfall intensity in the same circular ring. We use 7 rings "centered" at 25, 50, 65, 75, 85, 95, and 105 km. Rings are 10 km wide, but the 1st and 2nd ones that are 30 and 20 km wide. In this way, all rings have approximately the same area. There are three "small" differences between the present analysis in Israel and the original work by Gabella et al. (2006) in the Cyprus island: 1) the rings were all 10 km wide; 2) the maximum range used was 120 km; 3) the GR versus TPR comparison was based on the average linear radar reflectivity, $[Z] = \text{mm}^6 / \text{m}^3$.

With such large area rings ($\sim 6000 \text{ km}^2$), the volumes used to determine the averages are large, even much larger than the rather coarse TPR pulse volume resolution. The very large volume used for assessing average values, reduces mismatches in space (different geometry of observations, different horizontal and vertical resolution ...) and time. One effect of the beam divergence is a $1/r^2$ range-dependence that is already compensated in the radar equation. A second phenomenon is the influence of **non-homogeneous beam filling** in combination with the average **decrease** of the **vertical reflectivity profile with height**, which is the focus of this paper. As an example, at longer ranges of the GR, the lower part of the volume could be in rain, whereas the upper part of the same pulse could be filled with snow, or even be without an echo. This influence becomes more important at longer ranges, since the scattering volume increases in size.

2.2 Methodology

Let Z be the radar reflectivity (in mm^6 / m^3) and R the rainfall intensity (in mm/h). A fundamental quantity for precise assessment of both Z and R is the drop size distribution (DSD), which is defined as the number of rain drops per unit volume in the diameter interval

*Corresponding author address: Marco Gabella, MeteoSwiss, via ai Monti 146, CH-6605, Locarno, Switzerland; e-mail: Marco.Gabella@meteoswiss.ch

δD . If precipitating hydrometeors in the radar backscattering volume were all spherical raindrops (which is almost never the case!) and the DSD could be described, to a good approximation, by an exponential DSD, then a simple power-law would relate Z to R . The first ever exponential DSD presented in a peer-reviewed paper and probably the most quoted one is the Marshall-Palmer (M-P) distribution. The power law derived using the exponential fit proposed in Eq. (1) and (3) of the famous paper by Marshall and Palmer (1948) is $Z = 296 \cdot R^{1.47}$. We have used the following rounded values $(Z/300) = R^{1.5}$ to derive the variable of interest, R , from the geophysical variable, Z , which is directly detected by the weather radar.

Let $\langle GR(D) \rangle$ and $\langle TPR(D) \rangle$ be values of average rainfall intensity, averaged in azimuth at distance D from the GR for both the GR and the TPR. (Obviously such average involves only regions without clutter and where both radars have good visibility). These two variables show similar behavior, except for the decreased sensitivity of the GR with distance. Factor $F(D) = \langle GR(D) \rangle / \langle TPR(D) \rangle$ is statistically explained using a regression between $\text{Log}(F)$ and $\text{Log}(D)$. In formulas:

$$F(\text{dB}) = 10 \cdot \text{Log}(F) = a_0 + a_D \cdot \text{Log}(D/D_0), \quad (1)$$

where the normalization coefficient, D_0 , is set to the intermediate value $D_0 = 40$ km.

3. STUDY REGION AND DATA DESCRIPTION

The Israeli C-band radar is located close to Tel Aviv airport and next to the sea. The radar site (Lat. 31.99°; Long. 34.90°), named Shacham, is at 42 m above-sea-level; the antenna tower is ~ 23 m. Fig. 1 in Morin and Gabella (2007) shows a digital elevation map of the country and the radar site: Israel's physiography consists of 3 main longitudinal strips: the coastal plain, the hilly regions (Galilee, Samaria and Judean Mountains), and the Jordan Rift valley. The hilly ridge east of the radar causes both ground clutter and beam blockage, which represent two major difficulties of radar rainfall estimation in complex terrain. The lowest elevation (1°) is obviously more affected than the second one (1.6°). Additional ground clutter areas surround the radar at closer ranges, up to ~25 km.

With the antenna focus at 65 mm and in standard refractivity conditions, the beam axis at ~1° elevation (the lowest scan) reaches an altitude of ~2700 m at a 110 km range, which is the maximum analyzed distance in this work. The beam axis of the 2nd scan (~1.6° elevation) reaches ~3700 m at 110 km range. The main features of the GR are listed in Table I of Gabella et al., 2006b (page 95). In this study, (2 μ s) echoes were transmitted with a pulse repetition frequency of 250 Hz. The raw reflectivity values were sampled using 1.4° intervals in azimuth and 1000 m radial resolution range-bins. Just like suggested by Morin and Gabella (2007), prior to any computation

and averaging (see Sec. 3.1), the radar reflectivity values were increased by 6 dB to compensate for system losses not thoroughly taken into account in the implemented conversion from received power (in dBm) to radar reflectivity (in dBZ).

Several remarkable thunderstorms have hit Israel in February and March 2003. By analyzing data from 199 available daily rain gauges, it was surprising to realize that since February the 1st to March the 27th at least one of them detected rain uninterruptedly. During such 55 rain days, the average (\pm st. deviation) rainfall amount has been 379 \pm 132 mm. The (min.) maximum value was (12) 743 mm. Such value is particularly impressive if related to the fact that almost half of Israel area has an annual rainfall of less than 200 mm / year. The present study focuses on the first three weeks of March 2003: among the 18 available TRMM overpasses, 5 were characterized by widespread precipitation. However, only 4 had enough rain at all ranges between 10 and 110 km from the GR site so that each ring contained a reasonable number of rainy pixels. Hence, the most robust assessment of bias and range dependence presented in Sec. 4 is based on the integral of four overpasses.

Fig. 1 presents the first overpass, which occurred on March 3, 2003 at 18:38 UTC. Note that most of the 3° \times 2.5° region is under the TRMM umbrella (central picture): the satellite swath scene is in fact ~240 km while the distance between the Nadir line and the GR site (black mark) is ~40 km. The left (right) picture shows the nearest-in-time GR image acquired at ~1.6° (1°) elevation: the left image is characterized by less strong nearby ground clutter, the right one by much better visibility at far ranges and sea clutter in the NW direction. Such general peculiarities can also be observed in the following Fig.(s) 2-5. Overshooting of precipitation by the 2nd elevation (left picture) is clearly evident in the vicinity of the Gaza stripe and in Syria, where cells are present in both TRMM and the GR lowest elevation images. In the SE direction severe beam occultation is evident at both elevations.

Fig. 2 shows the 1st overpass on March 3. TRMM did not detect any weather echo within the 1st ring (10-40 km range): hence, for this overpass we have rather not derived the regression coefficients (using 6 points only). Note also that almost half of the region is not under the TRMM umbrella because the large distance between the Nadir line and the GR site (~120 km; similar situation in Fig. 4).

Fig. 3 shows the "best" overpass from a rain-distribution point of view: considerable precipitation is present at all ranges. Again note complete beam occultation for the GR in the SE direction (Latitude < 31.5°; Longitude > 35.5°).

Also the overpass shown in Fig. 4 is characterized by remarkable precipitation. Here, it can be seen that especially for the 2nd elevation, "equivalent" Earth curvature alone (without beam occultation by relieves) causes severe overshooting in the NW direction. The quality of the 2nd elevation is much poorer than expected (far precipitation fields are not detected).

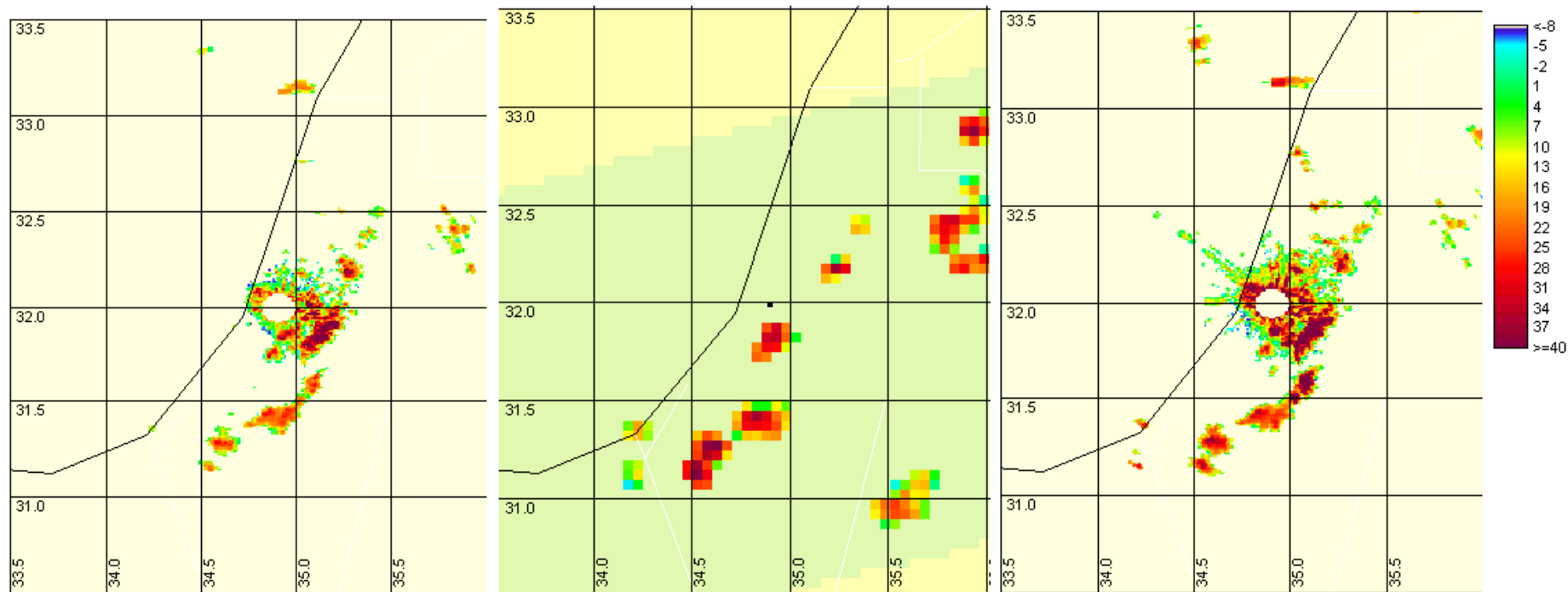


Figure 1. Complementary RADAR view of the highly variable (both in time and space) precipitation field over Israel on March 3, 2003. Colors represent radar reflectivity values in dBZ. The CENTRAL picture has been acquired from space (~402 km altitude) by the first ever spaceborne weather radar onboard the TRMM platform; the vertical resolution (~250 m at the Nadir) is much better than the horizontal one (~ 5 km diameter); because of the observation geometry, the spaceborne radar can collect weather echoes nearly with the same sampling volume resolution at any place of the swath scene. On the contrary the Ground-based Radar (GR) has to measure weather echoes from close to large distances. Consequently, the GR backscattering volume changes significantly within the surveillance area; the extent of blurring with range is indeed severe, since the sampling volume increases with the square of the distance from the GR site. The RIGHT picture refers to the 1st GR elevation (between 0.7° and 1.1° elevation) and has been acquired at 18:39 UTC. The LEFT picture refers to the 2nd GR elevation (between 1.4° and 1.7° elevation) and has been acquired at 18:40 UTC. The TRMM overpass, with ~40 km distance between the TRMM ground-track line at the Nadir and the “Shacham” GR site (black dot in the CENTRAL picture), took place at 18:38 UTC (orbit # 30203). Note that “no weather echo” (i.e., below sensitivity) is depicted in light (yellow) green in the (GR) TPR images.

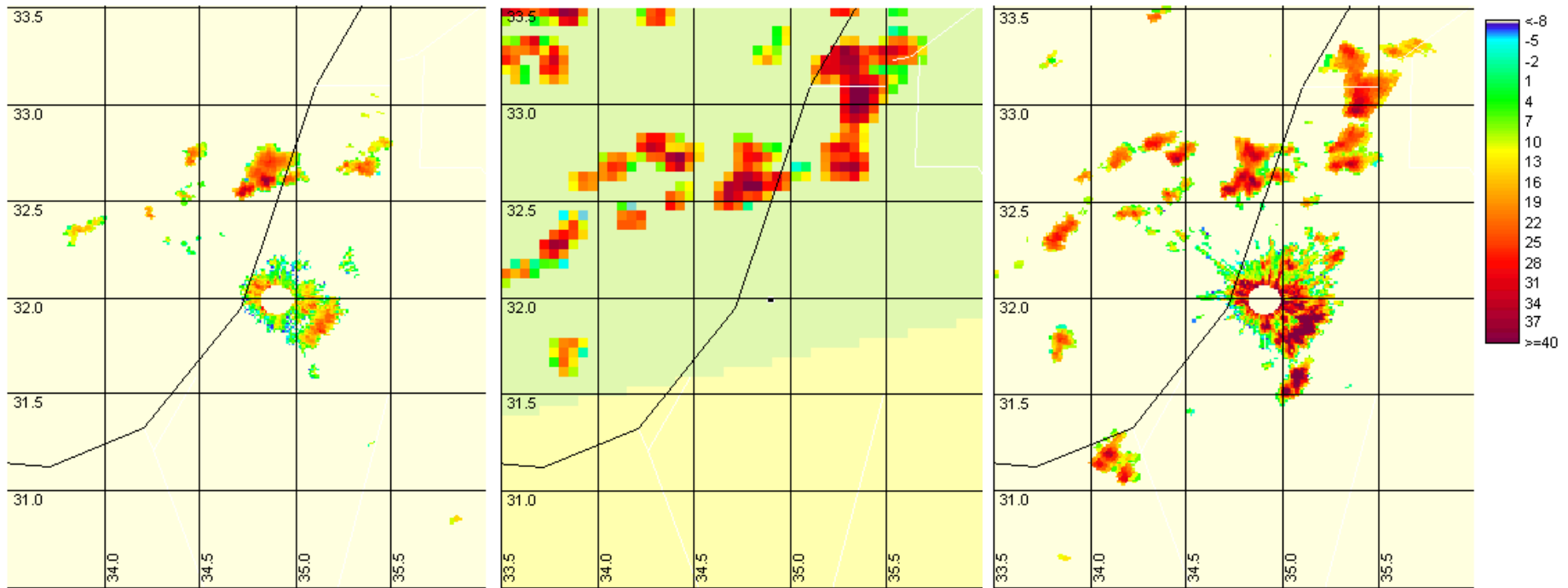


Figure 2. Same as Fig. 1 but for the first overpass over Israel on March 6, 2003. The RIGHT picture, which refers to the 1st GR elevation scan, has been acquired at 17:30 UTC. The LEFT picture, which refers to the 2nd GR elevation, has been acquired at 17:31 UTC. The CENTRAL picture shows the view from space: the TRMM overpass (~120 km distance between the TRMM ground-track line at the Nadir and the “Shacham” GR site - black dot), took place at 17:29 UTC (orbit # 30249). Note that “no weather echo” (i.e., below sensitivity) is depicted in light (yellow) green in the (GR) TPR images. Radar reflectivity values are in dBZ.

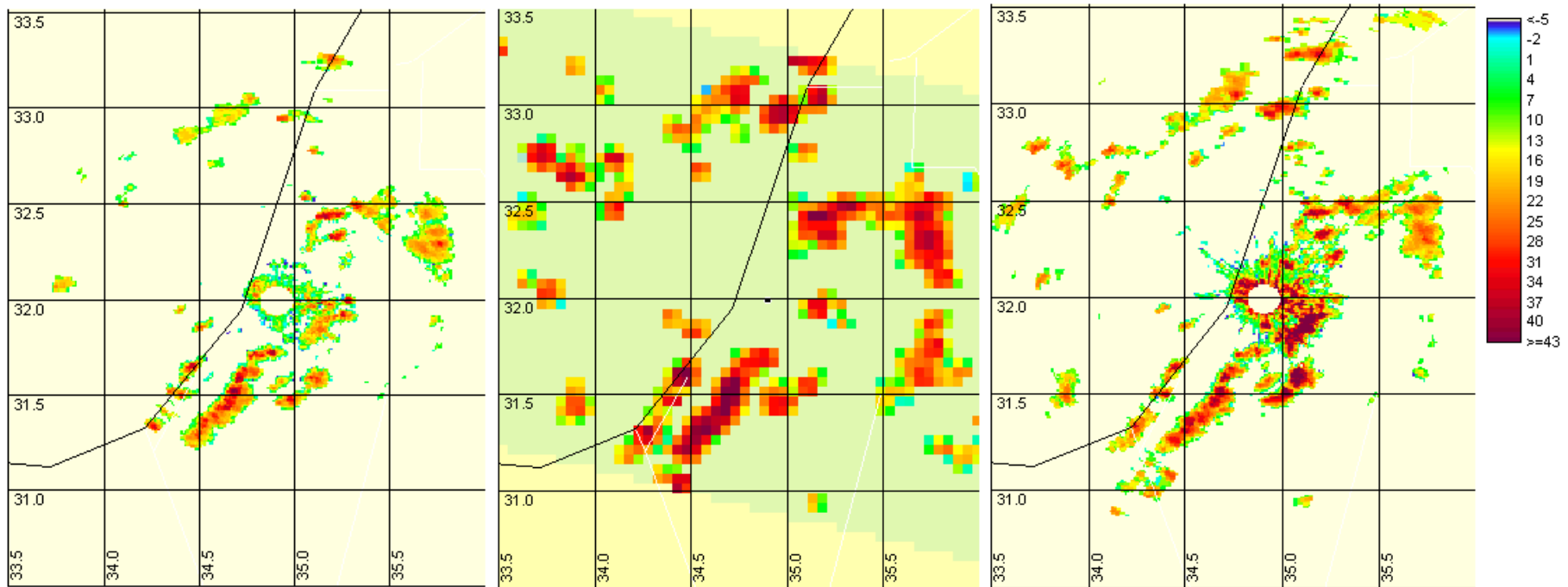


Figure 3. Same as Fig. 2 but for the second overpass over Israel on March 6, 2003. The RIGHT picture, which refers to the 1st GR elevation scan, has been acquired at 20:43 UTC. The LEFT picture, which refers to the 2nd GR elevation, has been acquired at 20:44 UTC. The CENTRAL picture shows the view from space: the TRMM overpass (~20 km distance between the TRMM ground-track line at the Nadir and the "Shacham" GR site - black dot), took place at 20:45 UTC (orbit # 30251). Note that "no weather echo" (i.e., below sensitivity) is depicted in light (yellow) green in the (GR) TPR images. Radar reflectivity values are in dBZ.

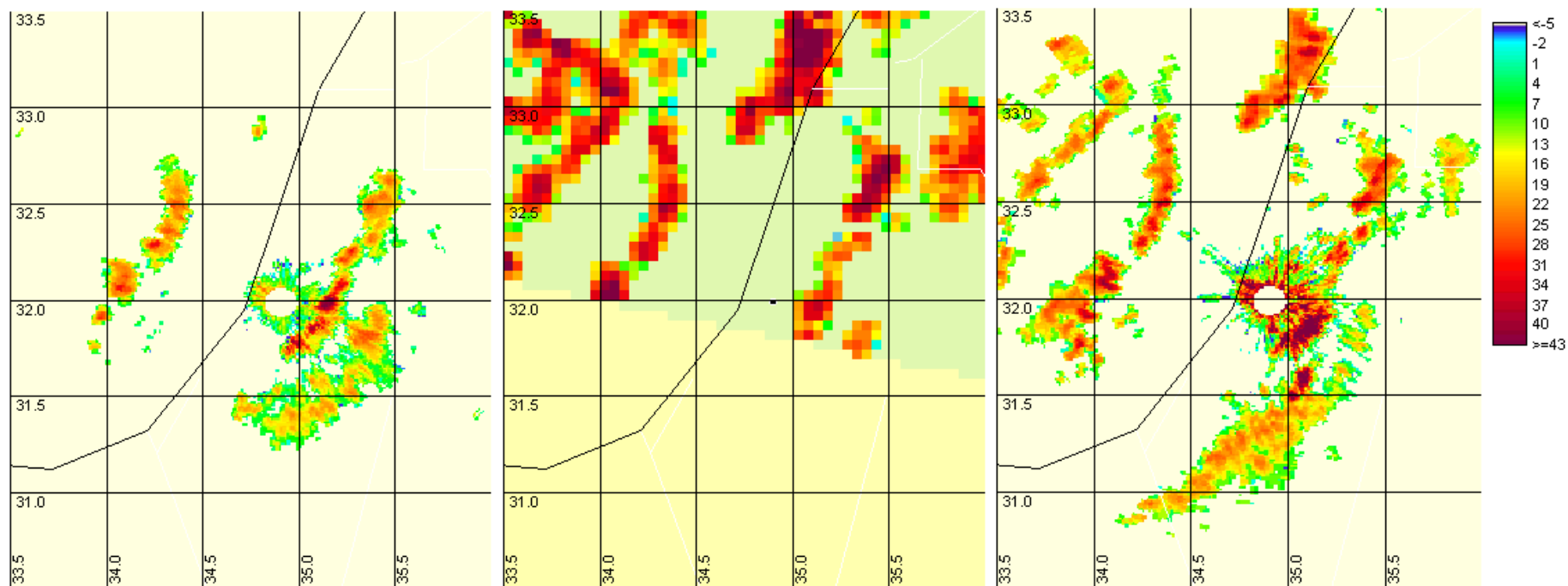


Figure 4. Same as Fig. 1 but for March 18, 2003. The RIGHT picture, which refers to the 1st GR elevation scan, has been acquired at 14:30 UTC. The LEFT picture, which refers to the 2nd GR elevation, has been acquired at 14:31 UTC. The CENTRAL picture shows the view from space: the TRMM overpass (~120 km distance between the TRMM ground-track line at the Nadir and the “Shacham” GR site - black dot), took place at 14:31 UTC (orbit # 30434). Note that “no weather echo” (i.e., below sensitivity) is depicted in light (yellow) green in the (GR) TPR images. Radar reflectivity values are in dBZ.

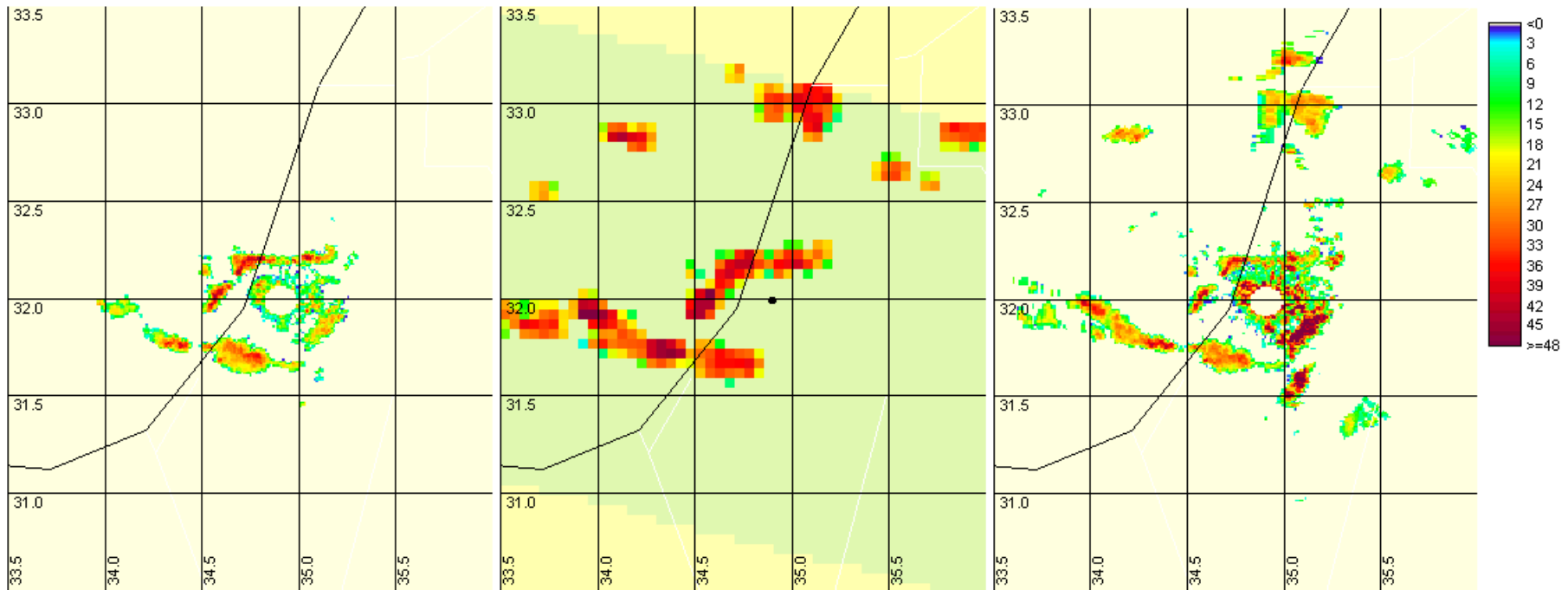


Figure 5. Same as Fig. 1 but for March 21, 2003. The RIGHT picture, which refers to the 1st GR elevation scan, has been acquired at 14:30 UTC. The LEFT picture, which refers to the 2nd GR elevation, has been acquired at 14:31 UTC. The CENTRAL picture shows the view from space: the TRMM overpass (~20 km distance between the TRMM ground-track line at the Nadir and the “Shacham” GR site - black dot), took place at 14:31 UTC (orbit # 30480). Note that “no weather echo” (i.e., below sensitivity) is depicted in light (yellow) green in the (GR) TPR images. Radar reflectivity values are in dBZ.

Fig. 5 confirms our concern regarding the 2nd elevation: again precipitation fields at ranges of ~ 100 km are surprisingly completely missed (for instance, remarkable precipitation is clearly visible in the central and right picture northern than 32.5°; on the contrary, no echo is present in the left picture).

4. RESULTS

The slope a_D in Eq. (1) reflects the deviation of the actual radar sensitivity from the theoretical $1/r^2$ law, which would require angular resolution independent of range and constant vertical reflectivity profile. So, negative slope values can be expected and were in fact found in Cyprus using 4 overpasses in February 2002 and 2003 (Gabella et al., 2006a). Here the analysis has been repeated in Israel using the 4 “suitable” rainy overpasses during the first three weeks of March 2003. Results for the 1st (~1° elevation) and 2nd scan (~1.6° elevation) of the GR are presented in Tables 1 and 2.

Table 1. Range-adjustment of the GR lowest scan derived using TPR images as reference (March 2003).

# of over-passes	TRMM orbits #	a_0 (dB)	a_D (dB/decade)	r^2 (%)
Two	30203, 30251	+1.6	-6.4	85%
Three	30434 added	+1.7	-6.1	92%
Four	30280 added	+2.1	-6.8	89%

Table 2. Range-adjustment of the GR 2nd scan (~1.6°) derived using TPR images as reference (March 2003).

# of over-passes	TRMM orbits #	a_0 (dB)	a_D (dB/decade)	r^2 (%)
Two	30203, 30251	+0.4	-10.6	90%
Three	30434 added	+0.9	-13.8	93%
Four	30280 added	+0.8	-13.8	89%

By increasing the number of couples of simultaneous GR and TPR images analyzed is a way to make the retrieval of the coefficients more robust. In this sense, the retrieved values shown in the last line of Tables 1 and 2 are likely the “best” ones. Also with the Israeli radar negative slopes are found. As expected, the 2nd elevation is much more affected by overshooting: the large underestimation with range found seems to confirm that Quantitative Precipitation Estimation up to 110 km using ~1.6° elevation is not feasible. Using 1° elevation, the adjustment factor, F_{dB} , as a function of the Logarithm of the distance from the radar site, is ~7 dB/decade. This means that, according to the TPR, when increasing the GR range from 10 km to 100 km, GR-derived rainfall intensity should be compensated by a factor of 5!

5. SUMMARY AND ONCLUSIONS

The radar sampling volume increases with the square of the range, which is often referred to as beam broadening. If the hydrometeors were homogeneously

distributed within the sampling volume, beam broadening would have no effect on the radar measurements. However, this is rarely the case. On average, the vertical radar reflectivity profile tends to decrease with height. Because of the Earth’s curvature, the larger the range is, the higher the radar sampling volume becomes. Consequently, a possible cause of the systematic range dependence of the ground-based radars is the old, well-known problem of overshooting, which, combined with the vertical decrease in the radar echo, can lead to serious underestimation.

This work illustrates the possible causes of the apparent decrease in sensitivity of the GR with range and presents a procedure that can be used to assess and eventually compensate the residual range dependence, using the radar in space as a reference. The TRMM radar offers the unique opportunity of validating ground-based radars. The developed algorithm permits a quantitative comparison between TRMM radar and any ground-based radar worldwide. It is extremely valuable in a Global Precipitation Measuring perspective.

6. REFERENCES

- Bolen S.M. and V. Chandrasekar, “Methodology for Aligning and Comparing Spaceborne Radar and Ground-Based Radar Observations”. *J. Atmos. Ocean. Technol.*, vol. 20, pp. 647–659, 2003.
- Gabella M., J. Joss, S. Michaelides, and G. Perona, “Range adjustment for Ground-based Radar, derived with the spaceborne TRMM Precipitation Radar”, *IEEE Transactions on Geoscience and Remote Sensing*, vol. 44, 126-133, 2006a.
- Gabella M., L. Corngati, E. Morin, and G. Perona, “Combining multisource data observations: how to use the TRMM spaceborne weather radar to adjust meteorological radars at ground level”, *Proceedings of the 7th Int. Workshop on Precip. in Urban Areas*, St. Moritz, pp. 93-97, 2006b.
- Houze R.A., S. Brodzik, C. Schumacher, and S. E. Yuter, “Uncertainties in oceanic radar maps at Kwajalein and implications for satellite validation”, *J. Appl. Meteorol.*, vol. 43, pp. 1114-1132, 2004.
- Keenan T., E. Ebert, V. Chandrasekar, V. Bringi, and M. Whimpey, “Comparison of TRMM satellite-based rainfall with surface radar and gauge information”. *Preprints of the 31st Int. Conf. on Radar Meteorol.*, Seattle, WA, pp. 383-386, 2003.
- Liao L., R. Meneghini, and T. Iguchi, “Comparisons of rain rate and reflectivity factor derived from the TRMM Precipitation Radar and the WSR-88D over the Melbourne, Florida, site”. *J. Atmos. Ocean. Technol.*, vol. 18, pp. 1959-1974, 2001.
- Morin, E. and M. Gabella, “Radar-based quantitative precipitation estimation over Mediterranean and dry climate regimes”, *Journal of Geophys. Res.*, 112, D20108, doi:10.1029/2006JD008206, 2007.
- Marshall J.S. and W. Palmer, “The distribution of raindrops with size”, *J. Meteor.*, 5, 165-166, 1948.